Supplementary Materials for

Individualized prediction of heroin cue-induced craving using task-based EEG functional connectivity

This supplementary material includes as follows:

Supplementary Figures

◆ Fig. S1. The analytical workflow and independent validation for outcome prediction in heroin use disorder.

◆ Fig. S2. Within-group functional coupling reconfigurations of β-band PEC networks following targeted iTBS interventions.

◆ Fig. S3. The source activation differences under addiction-related cues between Post-iTBS and HUD baseline across dynamic time windows using paired-sample t-tests.

◆ Fig. S4. The PEC model under neutral cues demonstrates limited predictive efficacy for craving in the cue-induced craving task dataset.

◆ Fig. S5. The frequency specificity of the predictive model.

◆ Fig. S6. The predictive performance of β-band PEC models across dynamic time windows under addiction-related cues at HUD baseline and Post-iTBS.

◆ Fig. S7. The diagram illustrating participant inclusion/exclusion criteria, related to Table 1.

◆ Fig. S8. The correlation relationship between the raw baseline predictive network strength (x-axis) and the actual observed changes in craving scores.

◆ Fig. S9. The Machine learning analysis details.

Supplementary Tables

◆ Table S1. The networks and their corresponding ROIs.

◆ Table S2. The Clinical scales used in the study.

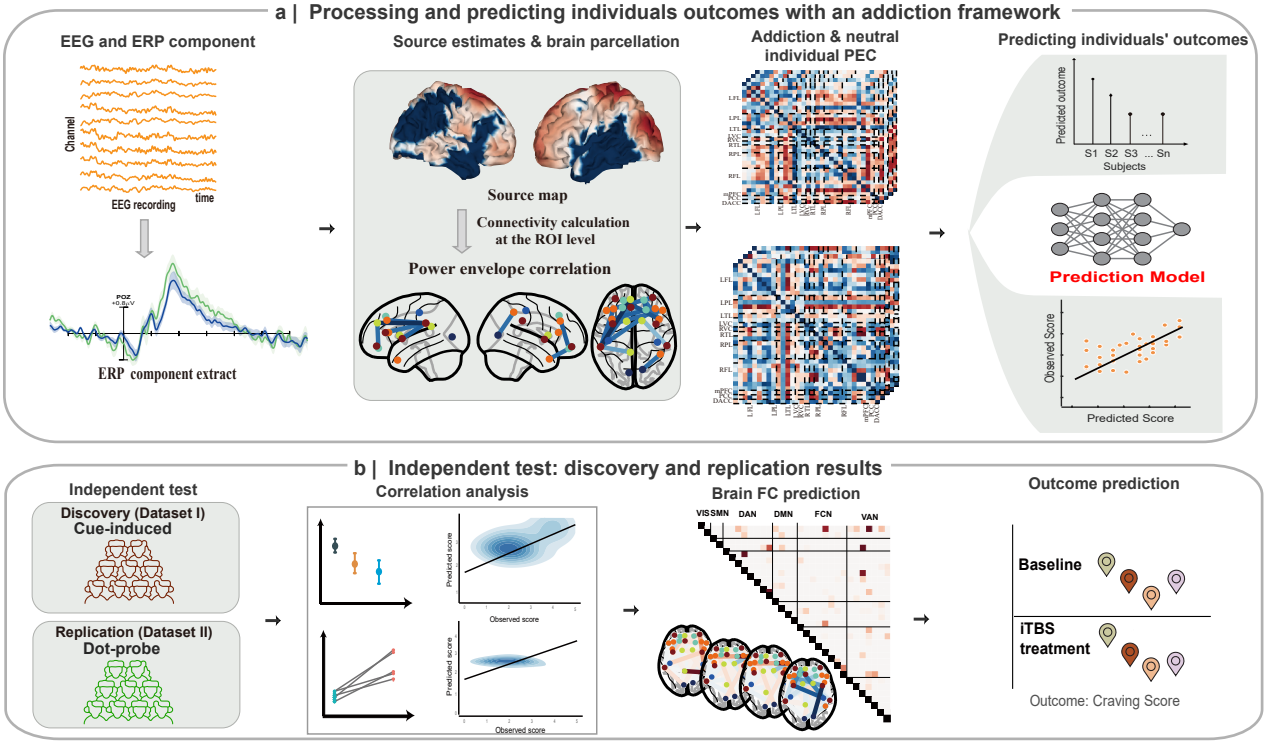


Figure S1: The analytical workflow and independent validation for outcome prediction in heroin use disorder. a) Processing steps including ERP component analysis, source estimation, and brain parcellation. b) Results from an independent cohort confirming the cue-induced craving task dataset and dot-probe task dataset.

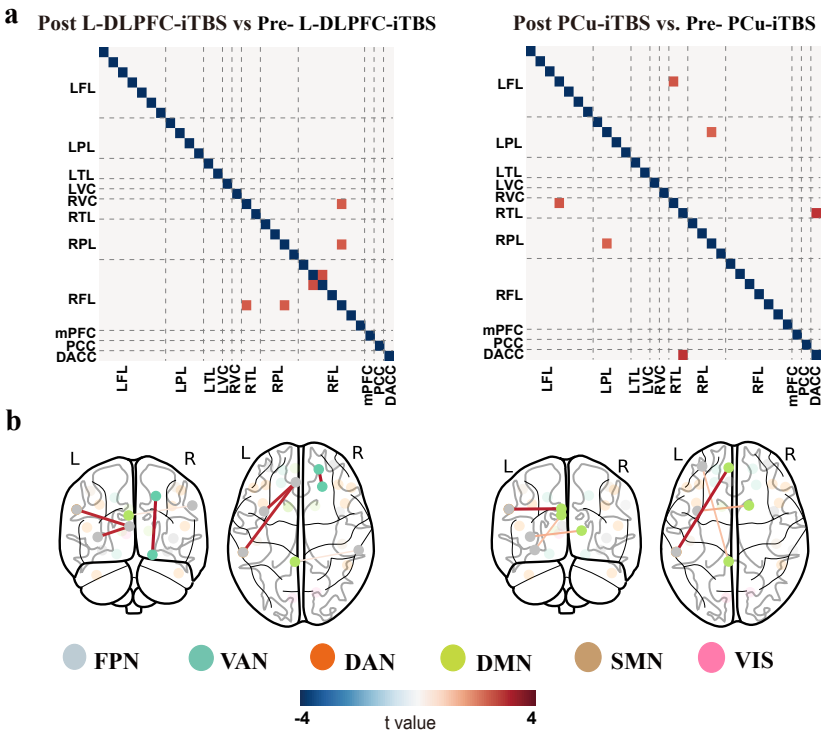


Figure S2: Within-group functional coupling reconfigurations of β-band PEC networks following targeted iTBS interventions. a) Regional-level functional connectivity matrices illustrating significant within-person changes following iTBS intervention for the L-DLPFC-iTBS and PCu-iTBS groups. Matrices are presented separately for the left dorsolateral prefrontal cortex (L-DLPFC-iTBS) and precuneus (PCu-iTBS) groups. For the L-DLPFC-targeted protocol, results indicate bolstered intrinsic connectivity within the right frontal lobe (RFL) and its functional links with the right temporal lobe (RTL) and right parietal lobe (RPL). In contrast, the PCu-targeted protocol facilitated increased coupling of the RTL with the left frontal lobe (LFL) and dorsal anterior cingulate cortex (dACC), while also augmenting connectivity between the RPL and left parietal lobe (LPL). Red squares indicate significantly increased functional connectivity post-intervention. b) Corresponding large-scale brain network visualizations mapping intervention-induced enhancements. L-DLPFC-iTBS significantly strengthened within-network connectivity of the frontoparietal network (FPN) and ventral attention network (VAN), as well as between-network connectivity between the FPN and the default mode network (DMN). In contrast, PCu-iTBS predominantly enhanced the connectivity between the FPN and DMN. Edges represent significant paired differences (paired t-test, $P < 0.05$). Nodes are color-coded according to their respective canonical large-scale networks.

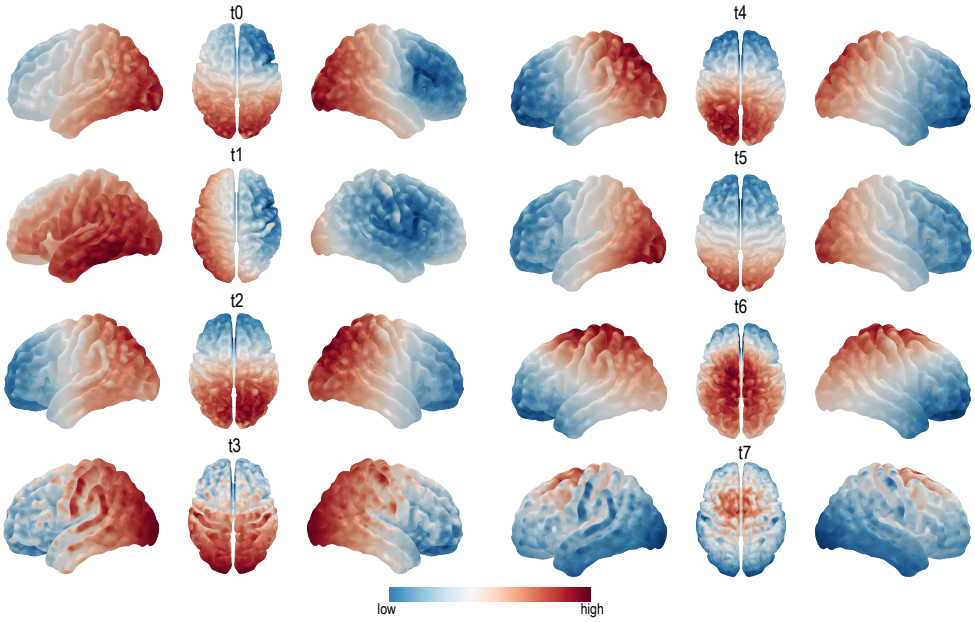


Figure S3: The source activation differences under addiction-related cues between Post-iTBS and HUD baseline across dynamic time windows using paired-sample *t*-tests.

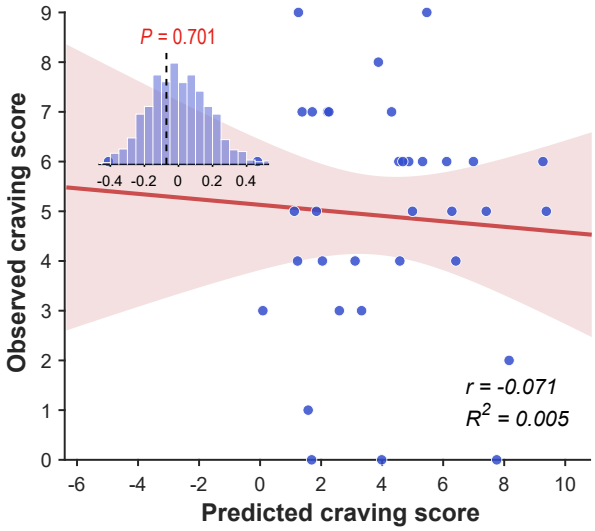


Figure S4: The PEC model under neutral cues demonstrates limited predictive efficacy for craving in the cue-induced craving task dataset ($N = 36$, $r = -0.071$, $P = 0.701$).

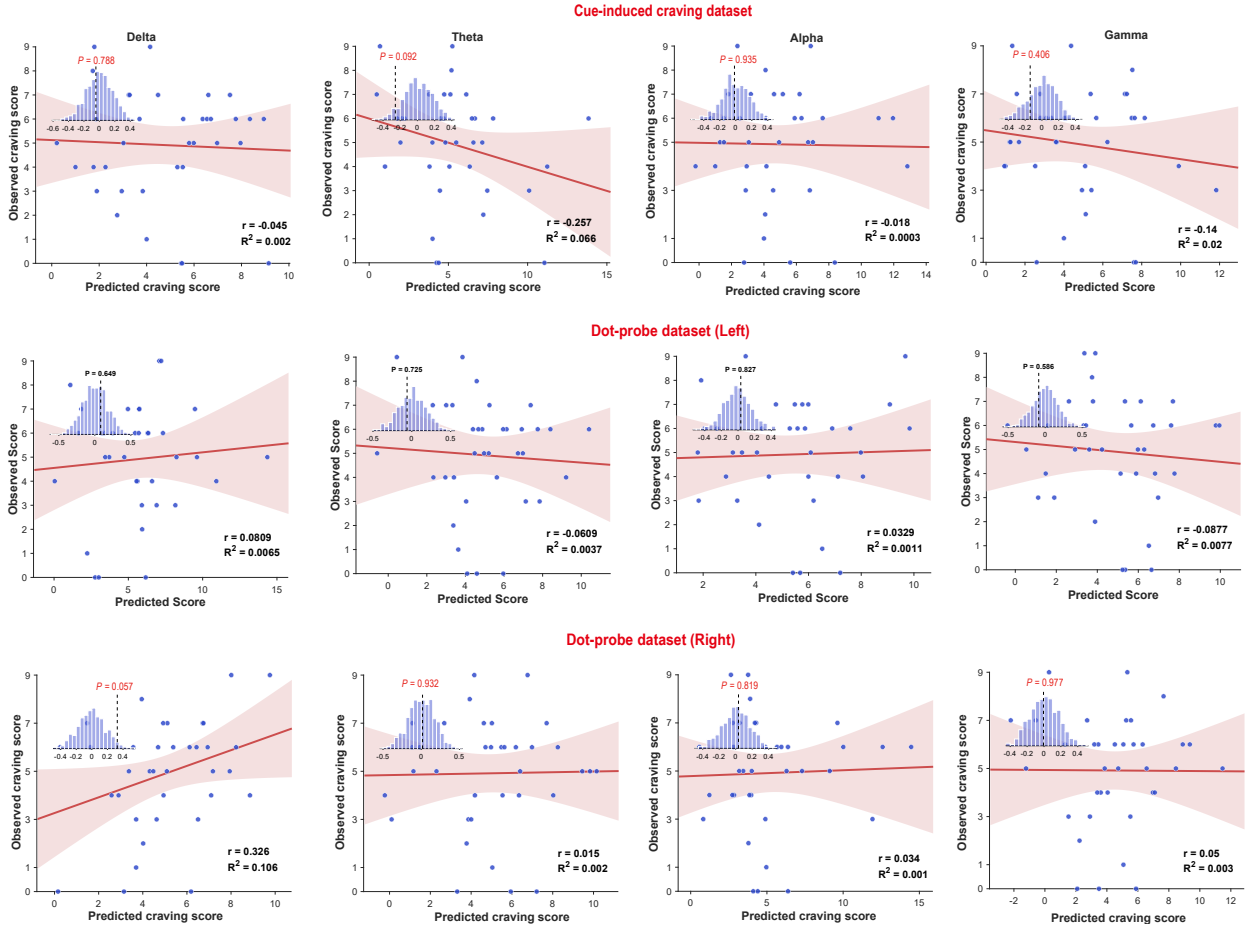


Figure S5: The frequency specificity of the predictive model. Scatterplots display Predicted versus Actual craving scores using PEC features extracted from non-β frequency bands (δ, θ, α, and γ). The red line indicates the linear regression fit with a pink 95% confidence interval. Inlay histograms show the permutation-based null distribution (1,000 permutations, light blue), with dashed black lines marking the observed Pearson's r and P-value. Across all non-β bands, models failed to reach statistical significance ($P > 0.05$).

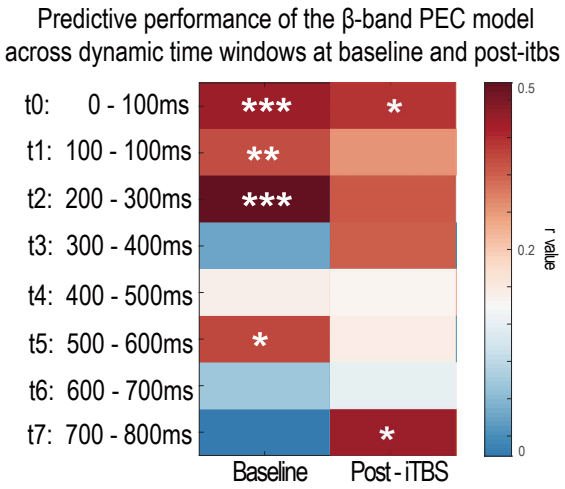


Figure S6: The predictive performance of β-band PEC models across dynamic time windows under addiction-related cues at HUD baseline and Post-iTBS. We evaluated the predictive performance of the β-band PEC models for craving scores across dynamic time windows at HUD baseline and Post-iTBS. The predictive efficacy is represented by r values. The statistical differences are represented by t-values. Significant results are marked with asterisks ($^{*}P < 0.05$, $^{**}P < 0.01$, and $^{***}P < 0.001$).

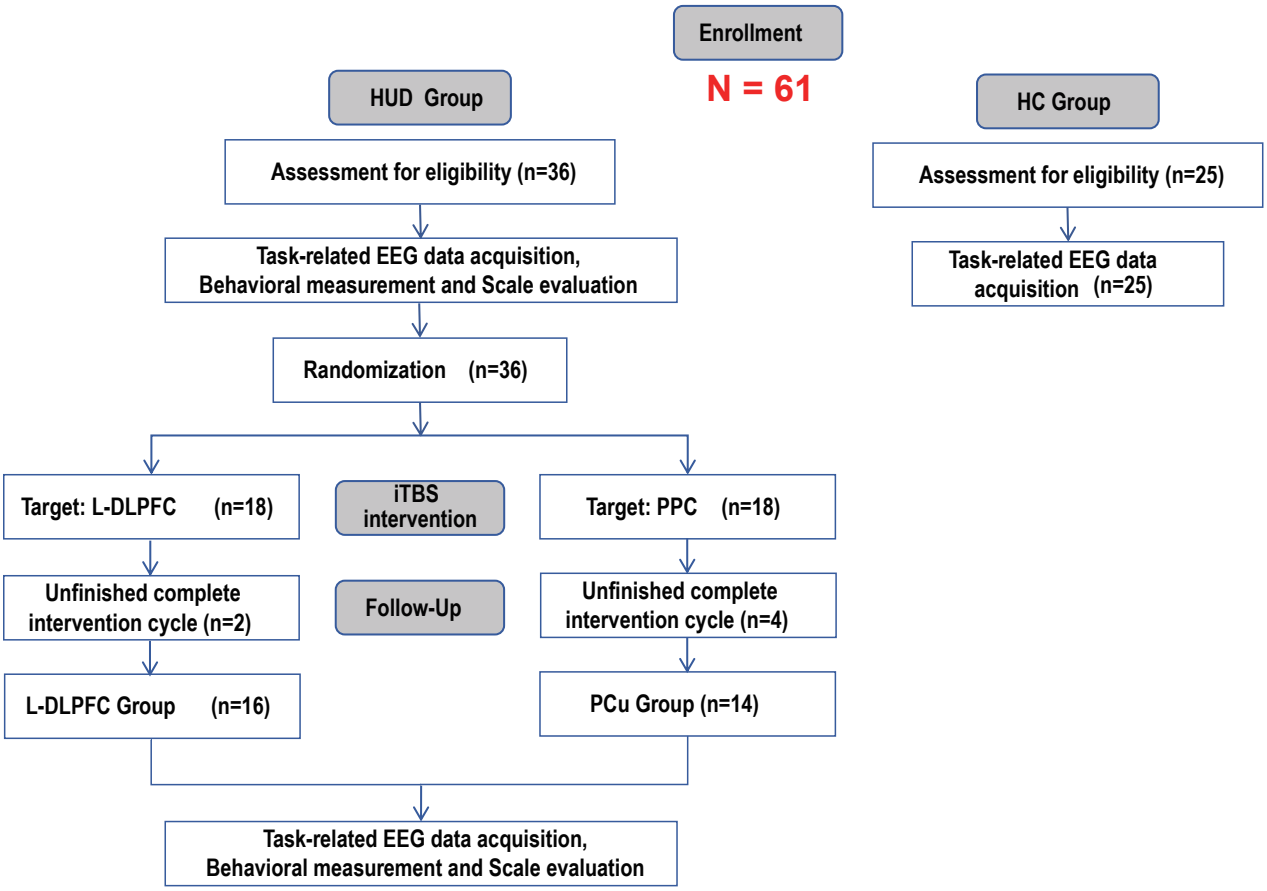


Figure S7: The diagram illustrating participant inclusion/exclusion criteria, related to Table 1.

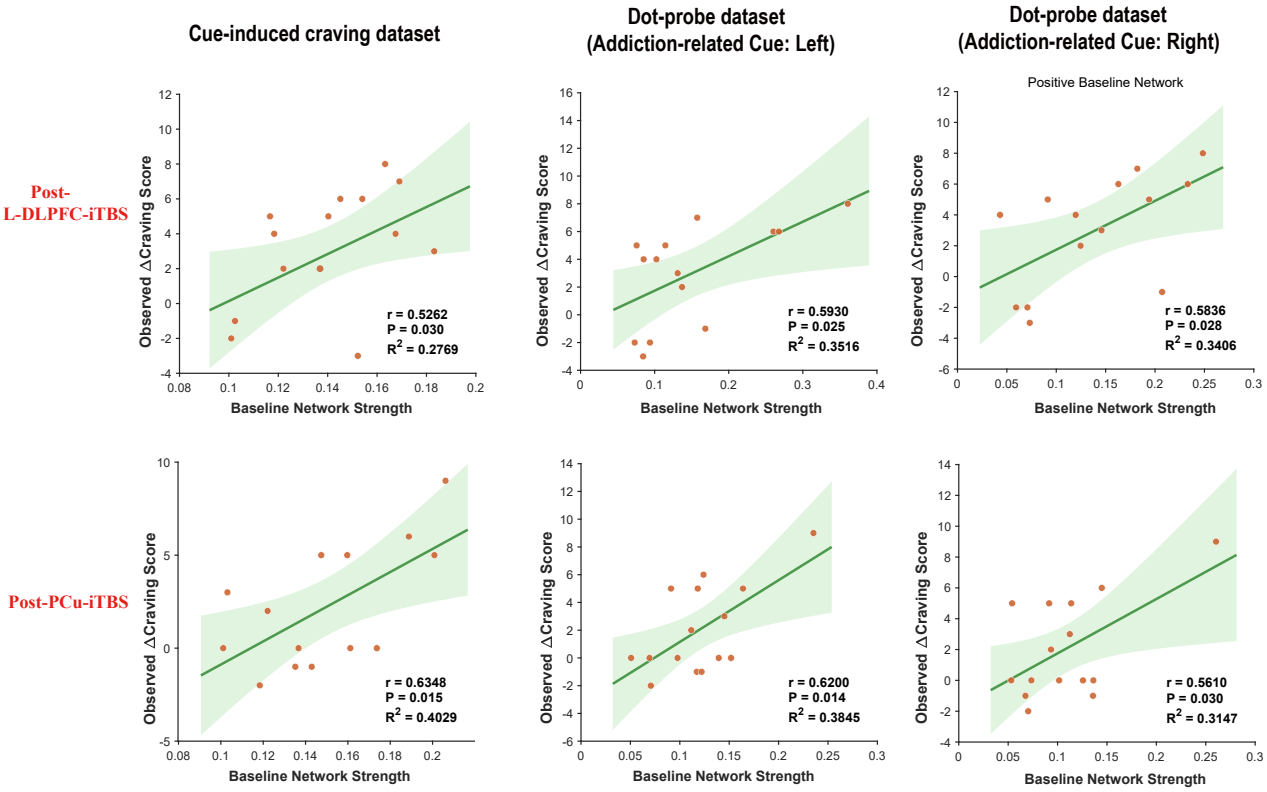


Figure S8: The correlation relationship between the raw baseline predictive network strength (x-axis) and the actual observed changes in craving scores (ΔCraving, y-axis). The solid green lines represent the linear regression fits, and the shaded regions indicate the 95% confidence intervals. The Pearson correlation coefficients (r) and significance levels (P) are annotated in each plot.

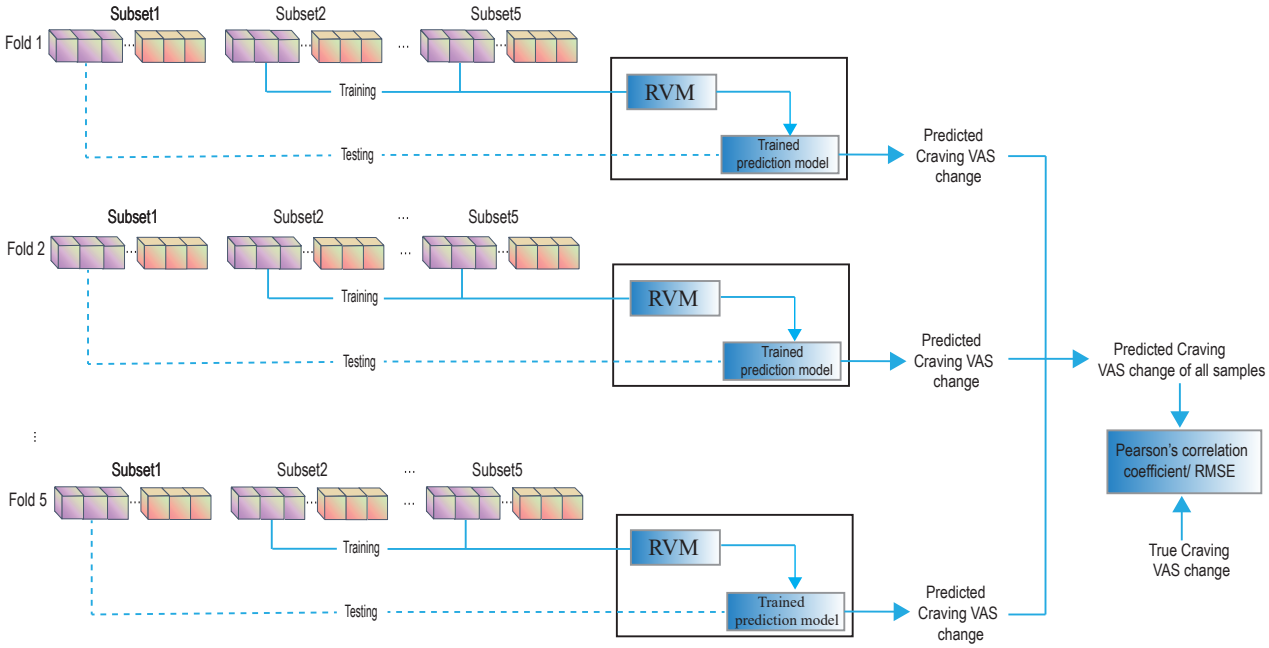


Figure S9: The Machine learning analysis details.

Table S1: The networks and their corresponding ROIs

Network	Regions of Interest (ROIs)
VIS	Visual Area 1 (V1)
SMN	Somatosensory Cortex (SMC)
DAN	Inferior Frontal Junction (IFJ), Intraparietal Sulcus (IPS), Frontal Eye Fields (FEF), Supplementary Eye Fields (SEF)
DMN	Posterior Cingulate Cortex (PCC), Medial Prefrontal Cortex (MPFC), Angular Gyrus (ANG)
FPN	Posterior Middle Frontal Gyrus (PMFG), Inferior Parietal Lobule (IPL), Orbital Gyrus (ORB), Middle Temporal Gyrus (MTG)
VAN	Anterior Middle Frontal Gyrus (AMFG), Insula (INS), Dorsal Anterior Cingulate Cortex (DACC), Supramarginal Gyrus (SUP)

Connectivity analysis was carried out on 31 regions of interest (ROIs) defined in the Montreal Neurological Institute (MNI) space, which were obtained from an independent parcellation of resting-state fMRI data based on the peak coordinates of ICA-derived clusters [1, 3]. For each ROI, the time series capturing the primary pattern of variability across all vertices within that region were computed using principal component analysis (PCA). To represent the ROI-level signal, we applied singular value decomposition (SVD) and took the first singular vector as the dominant component of the time series [2]. These 31 ROIs are divided into 6 networks: VIS (visual network): visual area 1 (V1); SMN (somatosensory network): somatosensory cortex (SMC); DAN (dorsal attention network). The specific brain region information is given in the table below.

Table S2: The Clinical scales used in the study.

Domain	Questionnaire	Description and measures derived
Emotion relevance (i.e., mental health)	PANAS (S-RQ)	Individuals' emotional states, comprising two dimensions: positive affect and negative affect
	PHQ-9 (S-RQ)	Sleep quality in individuals with mental disorders, primary insomnia, and the general population
	GAD-7 (S-RQ)	The severity of depressive symptoms in various patient populations.
	ERQ (S-RQ)	The frequency and habitual use of emotion regulation strategies, specifically cognitive reappraisal and expressive suppressi.
	TAS-20 (S-RQ)	The severity of alexithymia, encompassing three dimensions: difficulties in identifying feelings (DIF), difficulties in describing feelings (DDF), and externally oriented thinking (EOT).
Sleep	PSQI(S-RQ)	19 self-rated items and 5 clinician-rated items assessing sleep quality and disturbances over the past month.
	SCS(S-RQ)	individuals' sense of control, comprising two subscales: personal mastery and perceived constraintsendtabular
	RESE	The presence of generalized anxiety disorder in individuals.

Note: Self-Control Scale (SCS), Emotion Regulation Questionnaire (ERQ), Toronto Alexithymia Scale (TAS-20),Pittsburgh Sleep Quality Index (PSQI),Self-Control Scale (SCS), Positive and Negative Affect Schedule (PANAS).

References and Notes

[1] Ashley C Chen, Desmond J Oathes, Catie Chang, Travis Bradley, Zheng-Wei Zhou, Leanne M Williams, Gary H Glover, Karl Deisseroth, and Amit Etkin. Causal interactions between fronto-parietal central executive and default-mode networks in humans. *Proceedings of the National Academy of Sciences*, 110(49):19944–19949, 2013.

[2] Maria Rubega, Margherita Carboni, Martin Seeber, D Pascucci, S Tourbier, Giacomo Toscano, Pieter Van Mierlo, P Hagmann, G Plomp, Serge Vulliemoz, et al. Estimating eeg source dipole orientation based on singular-value decomposition for connectivity analysis. *Brain topography*, 32(4):704–719, 2019.

[3] Devarajan Sridharan, Daniel J Levitin, and Vinod Menon. A critical role for the right fronto-insular cortex in switching between central-executive and default-mode networks. *Proceedings of the National Academy of Sciences*, 105(34):12569–12574, 2008.